Probabilistic Models for Residual and Peak Transient Tilt of Mat-Founded Structures on Liquefiable Soils

Zach Bullock[1], Shideh Dashti[2]*, Zana Karimi[3], Abbie Liel[4], Keith Porter[5], and Kevin Franke[6]

Abstract: This paper presents models for predicting the residual and peak transient tilt of mat-founded structures on liquefiable ground. First, the study presents a completely empirical model based on correlating residual tilt to settlement in case histories. Second, a semi-empirical model for residual tilt is developed based on an extensive numerical parametric study of soil-foundation-structure systems, centrifuge tests performed by several researchers, and case history observations from several earthquakes. The model of peak transient tilt is based on centrifuge tests. The uncertainty around the estimates of each model is described using lognormal distributions, and all necessary correlation coefficients are calculated. The proposed procedure is the first methodology for estimating the residual tilt of such structures that is not derived solely from settlement models used to estimate differential settlement. It therefore accounts for the influence of complex phenomena (e.g., soil-structure interaction, asymmetric loading, inter-layering, and ejecta) that mechanistically affect tilt and settlement differently. The models consider various properties of the soil profile, foundation, and structure, and also characterize total uncertainty. These models constitute a fundamental component of a performance-based approach that could be combined with vulnerability functions in the future to evaluate liquefaction risks in terms of losses associated with tilt of structures.

[1] PhD Student, Department of Civil, Environ. and Archit. Engrg, Univ. of Colorado Boulder, 1111 Engrg Dr. ECOT 441, Boulder, CO, 80309; e-mail: zachary.bullock@colorado.edu
[2]* Associate Professor, Department of Civil, Environ. and Archit. Engrg, Univ. of Colorado Boulder, 1111 Engrg Dr. ECOT 514, Boulder, CO, 80309; e-mail: shideh.dashti@colorado.edu
[3] Geotechnical Engineer, AECOM, 6200 South Quebec Street, Greenwood Village, CO, 80111; e-mail: zana.karimi@aecom.com
[4] Associate Professor, Department of Civil, Environ. and Archit. Engrg, Univ. of Colorado Boulder, 1111 Engrg Dr. ECOT 517, Boulder, CO, 80309; e-mail: abbie.liel@colorado.edu
[5] Research Professor, Department of Civil, Environ. and Archit. Engrg, Univ. of Colorado Boulder, 1111 Engrg Dr. ECOT 441, Boulder, CO, 80309; e-mail: keith.porter@colorado.edu
[6] Associate Professor, Civil and Environ. Engrg, Brigham Young Univ., 368P Clyde Building, Provo, UT 84602; e-mail: kevin_franke@byu.edu

INTRODUCTION

Liquefaction has been a major factor contributing to damage and losses in a number of recent and historical earthquakes. For example, the extent and severity of liquefaction, and its damaging effects observed in the 2010-2011 Canterbury earthquake sequence, have been extensively investigated and documented (Cubrinovski et al. 2011a,b; Quigley et al. 2013; Bray et al. 2014). Likewise, the 2010 Chile earthquake and the 1999 Kocaeli and Düzce earthquakes provided a relatively large number of case histories of liquefaction-induced soil and structural damage (Bray and Sancio 2009; Unutmaz and Cetin 2010; Bertalot et al. 2013). Among the many consequences of liquefaction, damage associated with permanent settlement and tilt of structures is particularly costly, motivating efforts to develop design and remediation strategies that can potentially reduce these effects. Statistical models for predicting liquefaction-induced settlement of shallow-founded structures have recently been developed (Unutmaz and Cetin 2012; Bray and Macedo 2017; Lu 2017; Bullock et al. 2018). However, predictive models for the tilt of foundations on liquefiable soils that can be used as part of the design and decision-making processes are not readily available. This paper presents models for both the residual and peak transient values of foundation tilt.

The past several decades have seen the extension and refinement of predictive tools for liquefaction susceptibility (Bray and Sancio 2006), deterministic and probabilistic evaluation of triggering (Youd et al. 2001; Seed et al. 2003; Boulanger and Idriss 2014), and deterministic estimates of free-field (Tokimatsu and Seed, 1987; Ishihara and Yoshimine 1992) and foundation settlements (Liu and Dobry 1997). Motivated by the rising popularity and increasing maturity of performance-based design and decision-making methods, the most recent of these tools provide probabilistic estimates of settlement in the free-field (Cetin et al. 2009, 2012) or under a foundation (Unutmaz and Cetin 2012; Bray and Macedo 2017; Lu 2017; Bullock et al. 2018). A number of studies have also developed and evaluated indices and metrics that represent the vulnerability of a site to liquefaction, such as the liquefaction potential index and severity number (e.g., Maurer et al. 2014; Van Ballegooy et al. 2014).

Yet, the triggering of liquefaction, its surficial manifestations, and the corresponding settlement of the ground or foundation do not represent the full range of consequences of the phenomenon on structures.

45 The tilt of shallow-founded structures has also proved to be a significant driver of losses due to liquefaction.
46 Often, the only course of action for structures with severe residual tilt following an earthquake is demolition
47 (Bray et al. 2014), regardless of the performance of the structure itself. Residual tilt can also have a
48 dominant influence on insurance decisions. In addition, the transient tilt of a foundation (i.e., the tilt during
49 shaking) may affect the performance of the superstructure by amplifying P-Δ effects and nonlinear demands
50 (Paramasivam et al. 2018), or by damaging lifeline connections to the building, even if the residual tilt is
51 acceptable.

52 Previous studies have proposed the application of settlement models to estimate a foundation's
53 residual tilt (e.g., Bray and Macedo 2017). In this approach, the engineer estimates settlement of the
54 structure according to the soil profiles at either side of the mat foundation based on a given settlement
55 procedure, finds the difference, and uses foundation width to convert that differential settlement into an
56 estimate of foundation tilt or distortion. These estimates of tilt implicitly assume that foundation tilt or
57 differential settlement is solely a consequence of heterogeneity in the soil profile in plan. Vertical
58 heterogeneity and interlayering is accounted for only insofar as it affects the predictions of settlement,
59 which may not reflect its influence on tilt. Although soil heterogeneity is certainly a major contributor, tilt
60 (both transient and residual) is also a consequence of soil-foundation-structure-interaction (SFSI) induced
61 building ratcheting, as well as other complex phenomena in the underlying soil (e.g., ejecta), which depend
62 on the intensity, duration, and frequency content of ground motion as well as interlayering of the soil deposit
63 in elevation. This interaction means that residual tilt can occur even with a perfectly homogeneous site,
64 although estimates based on settlement procedures would always predict zero tilt in this case.

65 Figure 1 shows the average settlement and residual tilt of the mat-founded structures in a case
66 history database collected by the authors (detailed in Appendix I). Clearly, residual tilt is correlated to the
67 average foundation settlement, though not perfectly so. Yet, none of the soil profiles in these case histories
68 identify extreme soil heterogeneity in plan. Estimates of tilt based on differential settlement therefore
69 predict near zero tilt for these cases. Thus, a settlement-based prediction of tilt may be highly

unconservative, except for those cases where there is plan heterogeneity that is both observed and properly characterized.

Predictions of tilt based on differential settlement are also hampered by the fact that the relative importance of physical deformation modes for foundation tilt is expected to differ from that for settlement. Dashti et al. (2010a,b) and Adamidis and Madabhushi (2017) classified deformation modes that drive foundation settlement: shear type deformations under the static and dynamic loads induced by the building, volumetric deformations due to partial drainage, sedimentation, and consolidation, as well as soil ejecta. Shear deformations from SFSI-induced building ratcheting are intrinsically linked to transient tilt, and therefore to residual tilt, as well being important for settlement. In contrast, in the absence of substantial heterogeneity in plan, punching-type shear deformations under the building's static loads (due to softening) and certain volumetric deformation modes (e.g., partial drainage and sedimentation) likely have little effect on foundation tilt, despite their strong influence on settlement. Soil ejecta may also have a more significant effect on tilt compared to its effect on settlement. The heterogeneity of the soil profile in elevation is expected to affect the magnitude of ejecta and, hence, tilt (Beyzaei 2017). Uncertainties in tilt are also expected to differ from settlement, and this difference cannot be captured through a settlement-based approach.

This paper presents two probabilistic models for predicting the residual tilt of mat-founded structures. Motivated in part by Figure 1, the first is an empirical model describing residual tilt or foundation's angular distortion, expressed in degrees, as a function of settlement, based on case histories. As settlement is unknown for future earthquake scenarios, use of this model requires implementation in tandem of a probabilistic model for building settlement. The second, semi-empirical, model incorporates insights gained from a large numerical parametric study, databases of centrifuge tests, and case history observations. The numerical and centrifuge models did not consider soil heterogeneity in plan nor represent soil ejecta and effects of multi-dimensional shaking. Yet, the quality and quantity of these measurements made them valuable for developing a functional form for foundation tilt. Case history observations, on the other hand, included complexities of 3D heterogeneity, soil ejecta, and multi-dimensional earthquake

shaking, but their measurements were fewer in number and lower in quality. The resulting semi-empirical model is formulated to operate independently of any estimate of foundation settlement. Geometry and in-situ testing parameters, such as SPT or CPT with depth, are required for use of either model. Both models proposed in this paper yield probabilistic predictions for the foundation's residual tilt suitable for use in a performance-based framework. The paper also presents a model for peak transient tilt (based on its ratio with the residual tilt of the foundation, and, again, in units of degrees) from centrifuge results.

SIMPLIFIED EMPIRICAL MODEL FOR RESIDUAL TILT

Overview

In this section, we propose an empirical model for residual tilt based solely on case history observations. This model depends on the width of the mat foundation (B), the thickness of the non-liquefiable crust above the topmost susceptible layer in the soil profile ($D_{S,T}$), and the average settlement experienced by the foundation (S). Due to its development from case history observations, this model inherently includes the effects of SFSI-induced building ratcheting, 3D heterogeneity in soil, and ejecta on foundation tilt, to the extent that these phenomena occurred in the case history database. The goal of the proposed empirical model is to provide a relatively simple approach for predicting residual tilt, requiring only a prediction of settlement and minimal additional information (foundation size and profile geometry). However, this model requires co-implementation of a probabilistic model for foundation settlement, and the complexity and accuracy of this model depends on the relative complexity and accuracy of the embedded model for foundation settlement. We provide the necessary guidance to use this model in tandem with the Bullock et al. (2018) settlement model, which is reproduced in Appendix II, although other models may also be used (e.g., Bray and Macedo 2017).

Case history database

Table 1 summarizes the case history database of buildings with mat foundations on liquefiable soils used in this study (see also Appendix I). The same case history database was used as part of the development of the Bullock et al. (2018) model for foundation settlement. However, its extent is reduced here due to missing tilt measurements. Additionally, the two buildings with effective heights larger than 15 m were removed

from the database because these have a disproportionately large influence on regression coefficients. (Effective height is the height of a single-degree-of-freedom oscillator, typically taken as 70% of its true height if the structure is more than one story tall, and exactly its true height if it is one story tall.) We therefore limit the applicability of the model to structures with effective heights of 15 m or less, or roughly six stories or shorter.

Model development

The size of this database – $n = 20$ for mat-founded structures with recorded tilt values – necessitates a cross-validation based methodology for selecting a functional form. We consider the features listed in Table 2, considering properties of the ground shaking, soil, foundation, and structure.

In this table, S is the average foundation settlement, F_{LPC} is a flag that is 1 if the liquefiable material is below a low-permeability cap (e.g., a fine-grained deposit of plastic silt or clay with permeability less than approximately 10^{-7} m/s) and 0 otherwise, q is the foundation bearing pressure (kPa), B is the foundation width (smaller side of a rectangular mat foundation, m), h_{eff} is the effective height of the structure (m), M_{st} is the inertial mass of the structure (kg), D_f is the embedment depth of the foundation (m), $H_{S,1}$ is the thickness of the uppermost liquefaction-susceptible layer in the profile in meters, and $D_{S,T}$ is the depth from the ground surface to the top of the uppermost susceptible layer (considering only susceptible layers with some thickness >1m below the foundation). Susceptibility of soil to liquefaction (as relevant to $D_{S,T}$ and $H_{S,1}$) was evaluated according to the criteria of Bray and Sancio (2006), which is based on soil water content (w_c), liquid limit (LL), and plasticity index (PI) (a soil is susceptible if $PI \leq 12$ and $w_c/LL > 0.85$).

Here, we note that no additional information beyond those parameters listed in Table 2 regarding the density of the susceptible layers is needed. A factor of safety against liquefaction triggering has not been implemented in the proposed models, because triggering (e.g., defined as $r_u = 1.0$ or based on surficial manifestation of liquefaction) is complex under a foundation, and buildup of excess pore pressures and soil softening can cause notable seismic settlements and tilts of the foundation even without triggering. These factors are implicitly taken into account by including the properties of soil and loading imposed by the

structure and ground motion. However, additional information about susceptible layers and possibility of triggering may still be required if the co-implemented settlement model includes it.

Several intensity measures and locations for measuring these intensities (i.e., outcropping or within rock motion, far-field surface, or foundation) were considered. Cumulative absolute velocity (CAV) was previously selected as the optimum intensity measure (IM) for predicting foundation settlement by Bullock et al. (2018). Our analysis shows that a vector-valued IM containing CAV and either peak ground velocity (PGV) or peak incremental ground velocity (V_{gi}) of the outcropping rock motion is optimum (described in Appendix III). V_{gi} is defined as the absolute area under the largest acceleration pulse in a ground motion record (e.g., Jampole et al. 2016, Bullock et al. 2017). We select V_{gi} for potential inclusion, rather than PGV, because it offers slightly better efficiency and sufficiency. V_{gi} was also previously shown to outperform PGV in the context of base isolation (Jampole et al. 2016), a problem which has strong parallels with liquefaction (i.e., the inclusion of material at the base of a structure with relatively low stiffness). Perhaps counterintuitively, the intensity at outcropping rock sites is of interest because existing ground motion models (GMM) that include site effects are not applicable when liquefaction is expected (site behavior will be highly nonlinear, and site $V_{S,30}$ may be below the range of applicability). For all IMs, we use the maximum horizontal rotated component of the recorded ground motion ($RotD100$) because geotechnical site response is governed by the maximum shaking regardless of orientation, and is not orthogonal (i.e., as would be implied by the use of a geometric mean) (Cubrinovski et al. 2003). GMMs from Bullock et al. (2017) are therefore convenient because they used the maximum rotated component ($RotD100$) and focused specifically on IMs at rock sites. However, other GMMs can be used to predict outcropping rock motion by inputting an artificial rock outcrop shear wave velocity in place of $V_{S,30}$. The values of CAV and V_{gi} used for each case history are the deterministic median values predicted by the Bullock et al. (2017) GMMs. The need to use predictions from a GMM arises from a lack of outcropping rock accelerogram data in the case history database.

We employ a greedy forward stepwise selection strategy for feature selection (Efroymson 1960). The greedy forward stepwise algorithm begins by fitting all models with one feature from Table 2, retains the feature with the optimum validation error, and then fits all models with two features (one of which was carried from the previous step). This process repeats until eventually all features are selected.

We anticipate heteroscedastic model residuals because Figure 1 suggests that scatter in predictions of tilt appears to increase for larger values of settlement. As a result, we apply iteratively reweighted least squares (Holland and Welsch 1977), rather than ordinary least squares, to find model coefficients. We measure the quality of models based on the mean square validation error, which we estimate using leave-one-out cross-validation, or LOOCV (Stone 1974, Arlot and Celisse 2010). Figure 2 shows the LOOCV validation error, denoted MSE_V, for levels of complexity from 0 to 16 features. We select the model with 3 features, shown in Equation 1 and the coefficients provided in Table 3. The marginal improvement to model performance when adding a fourth feature is relatively small, and a fourth feature raises the possibility of over-fitting, given the size of the database.

The resulting functional form in Equation 1 and coefficients indicate that larger values of average foundation settlement (S), smaller foundation widths (B), and smaller thicknesses of the non-susceptible surficial crust ($D_{S,T}$) lead to larger values of residual tilt (θ_r). Dependence on shaking intensity is included implicitly in dependence on settlement. Settlement also reduces for larger values of $D_{S,T}$ (Karimi et al. 2018, Bullock et al. 2018); the inclusion of an additional term for $D_{S,T}$ in Equation 1 suggests that the influence of $D_{S,T}$ on tilt is not fully represented by its influence on settlement. The value of $D_{S,T}$ in a site investigation should be used without adjustment for the effects of any settlement that might occur during shaking.

$$\ln(\theta)_r = a_1 \ln(S) + a_2 \ln(B) + a_3 D_{S,T} + \varepsilon_{r^e} \quad (1)$$

The logarithmic residuals (i.e., natural logarithm of the observed value minus the natural logarithm of the predicted value) of this empirical model (ε_{r^e}) have a standard deviation (σ_{r^e}) of 0.29, and they pass the Lilliefors (1967) test for normality at the 5% significance level. Figure 3 shows the empirical model residuals as a function of the three predictor variables. Although we suspected heteroscedasticity on

settlement based on Figure 1, it is not evident in the model residuals. Heteroscedasticity with respect to B is apparent from inspection, particularly a decrease in the scatter near B of 12 m. Equation 2 provides a trilinear heteroscedastic characterization of model uncertainty,

$$\sigma_{r^e}^* = \begin{cases} \sigma_{r^e,1}, & B \leq B_1^* \\ \sigma_{r^e,1} - \left(\sigma_{r^e,1} - \sigma_{r^e,2}\right)\frac{(B-B_1^*)}{(B_2^*-B_1^*)}, & B_1^* < B \leq B_2^* \\ \sigma_{r^e,2}, & B_2^* < B \end{cases} \quad (2)$$

where B_1^* and B_2^* are threshold values of B that correspond to the values where heteroscedasticity is observed, with the parameter values reported in Table 3.

Model uncertainty

The values of $\sigma_{r^e}^*$ represent the "total uncertainty," rather than "model uncertainty," implicitly including uncertainty around all input parameters aside from S, insofar as these conditions are present in the case history database. Median values from the Bullock et al. (2017) GMMs are used in place of "true" ground motion intensity values, meaning that tilt predictions are essentially functions of magnitude, distance, and faulting characteristics, and uncertainty values presented in this study implicitly include uncertainty around ground motion intensity. However, a larger standard deviation may be observed if more case histories were available with a wider variety of SFS parameters, or capturing conditions not currently represented in the database. We use two bootstrapping techniques (wild bootstrap and case resampling) to generate two alternative descriptions of model uncertainty in Appendix IV (Wu 1986; Liu 1988). The resulting values of σ_{r^e} are approximately 0.34 and 0.38, respectively, compared to 0.29 from the model alone. If, alternatively, we combine our empirically-derived value with 0.25 through square root sum-of-squares, as suggested by FEMA P-58-1 Appendix H (FEMA 2012) when there is exogenous uncertainty (i.e., a case not covered in the model), a value of σ_{r^e} equal to 0.38 is estimated. If there is not exogenous uncertainty, 0.10 is suggested rather than 0.25, and the resulting value of σ_{r^e} is 0.30. The bootstrapping techniques presented in the appendix accomplish something similar to FEMA P-58-1.

One of the inputs to the residual tilt model is foundation settlement. In practice, this settlement is not known, and must be estimated from a predictive model. Substituting in the Bullock et al. (2018) model

for foundation settlement (Appendix II), one is left with the form shown in Equation 3. In this equation, $\ln(\bar{S})_{adj}$ is the natural logarithm of the median adjusted settlement provided by Bullock et al. (2018), and ε_S is its logarithmic residual (a normal random variable with zero mean and standard deviation, σ_S, of approximately 0.67). We show the contributions from uncertain ε_r and ε_S values separately to point out that ε_r and ε_S are correlated, and the total uncertainty ($\sigma_{r^e,tot}$) in Equation 4 depends on the correlation between these values. We calculate a correlation coefficient of 0.19 from the case history database used to develop this model of residual tilt.

$$\ln(\theta_r) = \alpha_1 \ln(\bar{S})_{adj} + \alpha_2 \ln(B) + \alpha_3 D_{S,T} + \varepsilon_r + \varepsilon_S \quad (3)$$

$$\sigma^2_{r^e,tot} = \sigma^2_{r^e} + \alpha_1^2 \sigma_S^2 + 2\alpha_1 \rho_{\theta_{r^e},S} \sigma_{r^e} \sigma_S \quad (4)$$

SEMI-EMPIRICAL MODEL FOR RESIDUAL TILT

Overview

In this section, we expand on the concept of the empirical model presented above by incorporating results from a comprehensive numerical parametric study and from available centrifuge experimental results, in addition to the case history database described previously. The resulting model may require more information about the SFS system compared to the empirical model presented previously, but the resulting model for tilt is now independent of an additional settlement model.

Numerical database

This second model for residual tilt takes advantage of 3D, fully-coupled, effective stress, dynamic numerical simulations conducted by Karimi et al. (2018), and summarized in Table 4. Figure 4 provides a schematic view of the models used in these numerical analyses. Over 420 models with varying soil, foundation, and structure properties were analyzed under a suite of 150 ground motions, resulting in more than 63,000 numerical case histories. Two of the authors previously calibrated and validated the models (Karimi and Dashti 2015, 2016). In the majority of simulations in this parametric study, Karimi et al. (2018) varied each input parameter separately, although a few input parameters were varied together, such as structure height with structure mass, and soil density with other parameters.

Results of the parametric study are summarized in Figures 5 through 8. Due to the extent of the database, we present results from selected ground motions only for clarity with details on these three motions provided in Table 5. The trends observed in the numerical results from these three ground motions are representative of the results from other, similar motions.

Figure 5 shows residual tilt as a function of several foundation parameters. As expected, the trends and underlying mechanisms for residual tilt can differ from those for foundation settlement (Karimi et al. 2018). At high intensities, bearing pressure (q) has a negative influence on tilt (despite its positive correlation with settlement at all intensities). Greater q amplify shear stresses transferred to the soil, but they also have a re-centering effect on foundations, reducing the foundation's tendency to accumulate rotation in one direction. At low intensities, increasing q slightly increased the foundation's cumulative tilt by amplifying shear stresses, while the re-centering effect was reduced due to smaller inertial effects. The foundation width (B) or foundation area (for a constant aspect ratio) also has a negative influence on tilt, and its influence is stronger than q. Wider foundations require larger differential settlements caused by ratcheting to undergo the same amount of tilt as narrower foundations. Further, for the same q, larger foundations have a larger zone of influence, increasing the confining pressure in a larger volume of soil. This is expected to increase the soil's stiffness and resistance to softening, which in turn reduce the mechanisms that contribute to foundation's tilt. In contrast, greater B tends to amplify average foundation settlement under stronger levels of shaking.

The foundation plan length-to-width ratio (L/B) also has a negative influence on tilt. Buildings with larger L/B ratios tend to undergo smaller permanent settlements and tilts on liquefiable soils, because drainage and shear strains become restricted primarily to the shorter dimension (B) and direction of shaking (approaching the 2D plain strain condition); in contrast, under square foundations, drainage and shear strains are effectively omnidirectional. Likewise, foundation embedment depth (D_f) tends to reduce tilt as it increases. This decrease is marginal when D_f < 3m, but more evident when it is increased from 3 m to 5 m for stronger levels of shaking. The soil neighboring the foundation is under a higher confining stress

when D_f increases, enhancing soil's resistance to foundation rotation, and the deeper foundation provides more area for SFSI to influence behavior.

Figure 6 shows the influence of various structural properties on residual tilt. Increasing structure height (h_{eff}) while keeping its aspect ratio (H/B) constant, has a negative effect on tilt, suggesting that the influence of foundation B overshadows the influence of h_{eff} in these results. This observation is reaffirmed by the apparent lack of a clear trend in tilt with respect to H/B with B held constant. The influence of h_{eff} may be intrinsically linked to the influence of inertial mass. Foundations of structures with greater inertial mass, M_{st}, experience larger overturning moments, contributing to increased ratcheting-type deformations and larger tilt. The vibration period of the structure (T_{st}) itself appears to have little influence on foundation's rotation (note that T_{st} was varied alone, i.e. without changes to h_{eff} or M_{st}).

Figure 7 shows the residual tilt as a function of soil profile parameters. The density of the uppermost susceptible layer, $D_{r,1}$, has a negative influence, but this trend manifests primarily as a sharp decrease in tilt between relative densities of 60% and 70%, with little change outside this range. Karimi et al. (2018) and Bullock et al. (2018) previously identified that a significant shift from contractive to dilative behavior occurs in this regime of relative density, influencing the extent of pore pressure generation and shear deformations below the foundation. Absent shear deformations, volumetric strains that are highly dependent on $D_{r,1}$ are expected to cause mostly uniform foundation settlement The thickness of the uppermost susceptible layer ($H_{S,1}$) has a positive, although slight, effect on tilt for thicknesses up to about 6 m, at which point the influence reduces significantly. The numerical model captures primarily deviatoric (shear) deformation modes, so this result suggests that once the susceptible layer is thick enough to fully engage shear mechanisms, adding more susceptible material has little effect.

Results in Figure 7 also show that deeper susceptible layers (farther from the foundation) are less influential. Based on these observations, we consider two measures of soil thickness: $H_{S,1.0B}$ and $H_{S,1.5B}$, defined as the thickness of susceptible material within $1.0B$ or $1.5B$ of the bottom of the foundation, respectively. (If a susceptible layer is cut by the threshold, the thickness below the threshold is excluded.)

Figure 7 also shows the sensitivity of foundation residual tilt to these parameters. Tilt increases with increasing $H_{S,1.0B}$, although this trend is dependent on intensity. Tilt also increases with larger $H_{S,1.5B}$, until $H_{S,1.5B}$ exceeds $H_{S,1.0B}$, after which point it plateaus or decreases. As a result, we select $H_{S,1.0B}$ will be the more useful parameter for predicting residual tilt.

There are a number of limitations to the numerical models. First, most SFS parameters were varied individually to allow for the separation of effects. However, this approach limits our ability to fully characterize interactions among parameters as they may influence tilt. Further, the numerical models do not consider heterogeneity of the soil properties in plan, are generally known to underestimate volumetric deformations, and may misrepresent or neglect the influence of void redistribution, strain localization, and soil ejecta on foundation deformations. The numerical results, therefore, only consider the contribution of shear mechanisms caused by the structure's pressure and inertia to the foundation's residual tilt. By not capturing large, cumulative shear deformations in the layered, softened soil profile below, these simulations produce soil behavior that is stiff relative to field behavior. As a result of these limitations, the numerical values of residual tilt are generally quite small. Nevertheless, because of its size, the numerical database is useful in evaluating trends, identifying the key parameters for predicting tilt, and developing a preliminary functional form for its prediction, subject to adjustment as described below.

Centrifuge experimental database

Due to inherent limitations of numerical modeling, we supplement the numerical results with results of centrifuge testing to better represent the effects of volumetric deformations and soil ejecta in the proposed semi-empirical model. Table 6 summarizes the centrifuge experimental database accessed by the authors. We include only tests of non-rigid, unmitigated structures (i.e., those with realistic dynamic properties and without drains, densification, or another form of liquefaction mitigation) on mat foundations over liquefiable ground (see also Appendix I).

In the centrifuge, each model is often subjected to multiple consecutive ground motions that build up in intensity (e.g., Dashti et al. 2010a,b). The permanent volumetric and shear strains in the soil, as well as permanent settlement and tilt of the foundation from earlier ground motions, have an important influence

on the behavior of the models in later ground motions. Therefore, we expect centrifuge test runs with little residual tilt remaining from previous shakes to be more realistic. In order to reduce the impact of tests with significant pre-existing tilt, we employ a weighting scheme shown in Equation 5 based on the initial overturning moment (M_{init}) and maximum overturning moment (M_{max}) for a given ground motion, where the overturning moment is calculated as the sum of moments due to horizontal accelerations of the masses ($\sum m_i h_i a_i(t)$) and moments due to P-Δ effects ($\sum g m_i \delta_i\,(t)$). In these equations, m_i is the i −th story mass, h_i is the height of the i −th story, $a_i(t)$ is the horizontal acceleration of the i −th mass, and δ_i is the horizontal deflection of the i −th story, including both flexural and rotational deformations. M_{init} represents the importance of residual tilt at the end of the previous motion. Tests where M_{init} is on the same order of magnitude as M_{max} are assigned zero weight, and tests with no initial tilt (i.e. M_{init} is zero) weighted as 1.

$$w = \max\left[1 - 10\left(\frac{M_{init}}{M_{max}}\right), 0\right] \qquad 5$$

Despite the advantages of centrifuge tests over numerical models in terms of capturing ejection behavior, scaling and use of viscous fluid may lead to differences between ejecta in the centrifuge and that in the field. In addition, the centrifuge experiments, like the numerical parametric study, used 1D horizontal shaking and soil profiles that are homogenous in plan and the variability and heterogeneity of soil layers in elevation was limited. Additionally, the idealized profiles in the centrifuge do not include certain factors that contribute to ejection, such as pre-existing cracks or weaknesses in impermeable layers arising from cycles of dessication not reproduced in the centrifuge. Hence, the centrifuge results still capture only a portion of total foundation tilt. The use of centrifuge test results in this context allows us to adjust the model to partially include the effects of ejection and to address specific limitations of numerical modeling (e.g., poor ability to capture sedimentation and inability to capture ejection), without combining these effects with those of soil heterogeneity.

Model development

We develop the semi-empirical model for residual tilt in three phases: (1) regression of a base model on the numerical database, (2) primary adjustment of the model according to centrifuge test results, and (3) secondary adjustment of the model according to the same case history observations (Appendix I. The case histories address the presence of heterogeneity, the differences in ejection behavior in the centrifuge and the field, as well as possible effects from more complex, multi-directional shaking. Appendix V provides a detailed, step-by-step description of this procedure. We apply lasso (Tibshirani 1996) to select features during phases (1) and (2). In phase (3), we evaluate proxies for vertical heterogeneity, and select features using greedy forward stepwise selection (as in the development of the first, empirical model).

Equation 6 shows the form selected for the base model, using the numerical database alone. All model coefficients are provided in Table 7.

$$\ln(\theta_r)_{num} = \alpha_0 + \alpha_1 \ln(q) + \alpha_2 \ln(B)^2 + \alpha_3 L/B + \alpha_4 \ln(L/B) + \alpha_5 \ln(D_f) + \left[\alpha_6 \ln(V_{gi}) + \alpha_7 \ln(CAV)\right] H_{S,1.0B} + \alpha_8 D_{S,1} + \alpha_9 H(17.2 - N_{1,60,1}) + \alpha_{10} \min\left(\frac{M_{st}}{10^6}, 1\right) + \alpha_{11}(H/B)\left(\frac{M_{st}}{10^6}\right) + \alpha_{12} \ln(V_{gi}) + \alpha_{13} \ln(CAV) + \varepsilon_{r,num} \quad (6)$$

In Equation 6, $\varepsilon_{r,num}$ are the logarithmic residuals following regression on the numerical database. We do not characterize $\varepsilon_{r,num}$ here because the model is subsequently adjusted further.

In Equation 6, $N_{1,60,1}$ is the SPT blow-count of the uppermost susceptible layer. The Heaviside step function, $H(\cdot)$, is essentially a flag that is 1 if the uppermost layer is sufficiently loose, and 0 otherwise. This term can be rewritten in terms of either CPT resistance or relative density as $H(140.2 - q_{c1N,1})$ or $H(70\% - D_{r,1})$, respectively, where $q_{c1N,1}$ and $D_{r,1}$ are the CPT normalized tip resistance and relative density of the uppermost susceptible layer. These values were determined using the relationships from Meyerhof (1957), Skempton (1986), and Idriss and Boulanger (2008), i.e.:

$$N_{1,60} = 35(D_r/100)^2 \quad (7)$$

$$q_{c1N} = 0.9\left(\frac{D_r/100 + 1.063}{0.465}\right)^{3.788} \quad (8)$$

368 The coefficients used in these relationships were developed based on laboratory tests, but subsequently
369 validated with NCEER field observations of liquefaction triggering (NCEER 1997).

370 Equation 6 showed significant systematic under-prediction when applied to the centrifuge test
371 results. This underprediction is attributed to the phenomena observed in the centrifuge that are not captured
372 sufficiently by the numerical models as described above, especially ejecta, sedimentation, and localized
373 shear and volumetric deformations within grains below the edges of the foundation that lead to accumulated
374 permanent rotation. Collinearity among certain parameters (i.e., q, M_{st}, and h_{eff}) also likely plays a role.
375 We used the lasso again to formulate a latent variable correction for this bias (Skrondal and Rabe-Hesketh
376 2004). Equation 9 provides the adjustment using the centrifuge database.

377 $$\ln(\theta_r)_{adj} = \ln(\theta_r)_{num} + \gamma_0 + \gamma_1 \ln(h_{eff}) + \varepsilon_{r,adj} \quad 9$$

378 All coefficients are provided in Table 7. The lasso selects effective height as the only parameter needed to
379 remove the bias from the numerically-based model. As before, $\varepsilon_{r,adj}$ is the logarithmic residual of predicted
380 residual tilt, but is irrelevant after phase 3 of the model development so is not further explored.

381 At this stage, the model does not fully incorporate the influence of 3D heterogeneity and ejecta
382 observed in the field, which are incorporated using the case history database. The effects of vertical
383 heterogeneity on tilt are uncertain and, likely, variable. A greater degree of interlayering between non-
384 susceptible, plastic, fine-grained soils and susceptible, non-plastic, granular soils within the foundation's
385 zone of influence may amplify void redistribution and shear strain localization (e.g., Kokusho 2003;
386 Malvick et al. 2006; Dashti et al. 2010b). This effect lowers shear resistance near the top of susceptible
387 layers, potentially amplifying foundation's tilt tendencies. In addition, greater interlayering may have mixed
388 effects on surface manifestation of sand ejecta, which influences deformations and tilt. On one hand, non-
389 susceptible interlayers may be subject to large hydraulic gradients resulting from the localization of large
390 excess pore pressures and void redistribution. These hydraulic gradients can increase their potential for
391 disturbance and fracture, which would increase the likelihood of ejection and its effects. Conversely, a
392 greater degree of interlayering might reduce tilt potential if the non-susceptible interlayers localize pore

pressures within thinner liquefiable layers, while resisting fracture and suppressing surface manifestation of ejection (e.g., Beyzaei et al. 2018, Cubrinovski et al. 2017). The potentially countervailing effects of interlayering are expected to depend on the properties of the soil profile and interlayers at a systems level (Cubrinovski et al. 2017) and ground motion characteristics. We expect to find a positive correlation between proxies for vertical heterogeneity and tilt if the increased softening due to void redistribution dominates the possible reduction in ejection, and a negative trend if otherwise.

We consider a wide range of proxies for vertical heterogeneity that influence the extent of void redistribution, ejection, and tilt, as detailed in Appendix VI. We select a combination of: (1) thickness of the largest continuous layer of susceptible material in the top B depth of the profile below the foundation ($\max(H_S)_{1.0B}$); and (2) the number of distinct non-susceptible layers per susceptible layer in the top B depth of the profile below the foundation ($N_{NS,1.0B}/N_{S,1.0B}$). In $\max(H_S)_{1.0B}$, adjacent layers are considered as a single layer if they are both susceptible or if they are both non-susceptible, even if they have other differences.

Equation 10 shows the final form selected for the secondary adjustment based on case history observations. Up until this point, we have used recorded values of outcropping rock CAV and V_{gi} from the numerical or centrifuge tests. However, we do not have acceleration data corresponding to the shaking experienced by the case histories, so we replace these values by the median predictions of the Bullock et al. (2017) GMMs.

$$\ln(\theta_{r^{se}}) = \ln(\theta_r)_{adj} + \kappa_0 + \kappa_1 F_{LPC} + \kappa_2 D_{S,T} + \kappa_3 \max(H_S)_{1.0B} + \kappa_4 \left(N_{NS,1.0B}/N_{S,1.0B}\right) + \varepsilon_{r^{se}} \quad 10$$

Here, $\varepsilon_{r^{se}}$ is the logarithmic residual of the final semi-empirical model, which has zero mean and standard deviation $\sigma_{r^{se}}$. These residuals pass a Lilliefors (1967) test for normality.

In Equation 10, $N_{NS,1.0B}/N_{S,1.0B}$ provides a direct proxy for coarse interlayering. The positive coefficient (κ_4) on this proxy suggests that the effects that increase tilt (e.g., amplification of void redistribution) outweigh the effects that might decrease it (e.g., possible reduction in ejection potential), at least insofar as these effects are present in the case history database. The observation that profiles with

418 larger values of $\max(H_S)_{1.0B}$ tend to produce smaller tilts is consistent (profiles with more coarse
419 interlayering tend to have thinner continuous layers of susceptible materials). Due to the resolution at which
420 soil profile data is available in the case history database, the smallest layer considered in our analysis is 1
421 m thick. We are therefore unable to capture the effects of very fine interlayering (i.e., lenses of sand on the
422 order of centimeters thick), and its impact is implicitly included in model uncertainty.

423 Figure 8 shows the residuals of this model as a function of several key parameters.
424 Heteroscedasticity may be apparent with respect to a few parameters (e.g., $D_{S,T}$ and $\max(H_S)_{1.0B}$), but there
425 are insufficient data in the extreme ranges of these parameters to confidently characterize it. This semi-
426 empirical model has a similar range of uncertainty when compared to the empirical model (Equation 1)
427 presented above, but it provides estimates that are independent of settlement. Note that Table 7 provides
428 the correlation between the errors of this model and the Bullock et al. (2018) model for settlement. This
429 correlation is not needed to produce predictions of tilt, but engineers can use it along with the Bullock et al.
430 (2018) settlement model to produce correlated probabilistic predictions of settlement and tilt.

431 **Model uncertainty**

432 As with the empirical model, the uncertainty ($\sigma_{r^{se}}$) represents "total uncertainty," and is suitable for use in
433 forward analysis.

434 **MODEL FOR PEAK TRANSIENT TILT**

435 **Model development**

436 Development of a model for the peak transient tilt of mat foundations (θ_{pt}) relies on centrifuge experimental
437 results, because transient tilt of mat-founded structures is not provided by case histories. This treatment of
438 the peak transient value of an engineering demand parameter (EDP) is not novel: structural engineers have
439 previously considered the ratio between peak transient and residual story drift ratios (Ruiz-Garcia and
440 Miranda 2006). Here, we define the *transient tilt ratio*, R_T as;

441 $$R_T = \frac{\theta_{pt}}{\theta_r} \qquad 11$$

We use the lasso to determine the functional form of the model for R_T, given by Equation 12, and explained in detail in Appendix V. Table 8 provides the coefficients for this model and characterizes its uncertainty. Model predictions for R_T should be left-truncated at 1.0, because smaller values are not physically possible. In this equation, ε_{R_T} is the logarithmic residual of predictions of R_T, which has zero mean and standard deviation σ_{R_T}, and θ_r is the observed value of residual tilt, meaning that it is an uncertain quantity in forward prediction (i.e., we do not know the observed θ_r before it occurs). Table 8 provides the correlation coefficient needed to characterize uncertainty around R_T when θ_r is predicted using the semi-empirical model in this study.

$$\ln(R_T) = \delta_0 + \delta_1 \ln(\theta_r) + \delta_2 \ln(B) + \delta_3 H_{S,1.0B} + \varepsilon_{R_T} \quad 12$$

Figure 9 shows the residuals of this model. These residuals also pass a Lilliefors (1967) test for normality. Heteroscedasticity is apparent with respect to the foundation width, and its characterization follows the same form as Equation 2, but with different coefficients, provided in Table 8.

The model for the transient tilt ratio suggests that increasing B makes the ratio of transient to residual tilt closer to one; for wider foundations, more energy is needed to re-center the foundation so the residual tilt is likely closer to the transient tilt. Increasing $H_{S,1.0B}$ increases the peak transient tilt; greater thickness of the liquefaction susceptible material within the foundation's zone of influence results in greater softening, amplifying building's ratcheting behavior and hence, the transient tilt ratio.

We expect this model of transient tilt ratios to be conservative. As discussed previously, the centrifuge results primarily reflect tilt due to inertial effects and localized volumetric strains. In the field, these tilts may be amplified by the presence of both vertical and horizontal heterogeneity in the site, as well as ejecta. However, these forms of tilt tend to accumulate in one direction and are unlikely to reverse. Therefore, the centrifuge database tends to estimate larger transient tilt ratios by its inherent bias toward more reversible components of foundation tilt. If these irreversible components of tilt dominate, the transient tilt ratio reduces to about 1.0 (when peak transient and residual tilts are similar in magnitude and direction).

Model implementation and uncertainty

Probabilistic estimates of peak transient tilt presented above considering uncertainties in residual tilt and the ratio predicted above. The correlation between ε_r and ε_{R_T} for the centrifuge results is -0.182. This correlation suggests that when we over-predict residual tilt, we tend to under-predict the transient tilt ratio. This trend is expected given that larger residual tilts should push R_T towards 1.0, which is its minimum value. However, this relationship is very weak, and this negative correlation reduces overall model uncertainty only slightly. The variance of the natural logarithm of peak transient tilt (σ_{pt}^2) is given by Equations 14 and 15. The heteroscedastic estimates of σ_r and σ_{R_T} (previously denoted as σ_r^* and $\sigma_{R_T}^*$) can be used in Equation 15 to generate a heteroscedastic estimate of σ_{pt} (which would be denoted σ_{pt}^*) depending on B. Note that the appropriate standard deviation of residual tilt needs to be used based on which model is being implemented (σ_{r^e} for the empirical model, or $\sigma_{r^{se}}$ for the semi-empirical model).

$$\ln(\theta_{pt}) = \ln(\theta_r R_T) = \ln(\bar{\theta}_r) + \varepsilon_r + \ln(\bar{R}_T) + \varepsilon_{R_T} \quad (13)$$

$$\sigma_{R_T,tot}^2 = \sigma_{R_T}^2 + \delta_1^2 \sigma_r^2 + 2\delta_1 \rho_{\theta_r,R_T} \sigma_r \sigma_{R_T} \quad (14)$$

$$\sigma_{pt}^2 = \sigma_r^2 + \sigma_{R_T,tot}^2 = (1 + \delta_1^2)\sigma_r^2 + \sigma_{R_T}^2 + 2\delta_1 \rho_{\theta_r,R_T} \sigma_r \sigma_{R_T} \quad (15)$$

Peak transient tilt predictions made with this model can be combined with estimates of flexural drift in the superstructure to estimate the total drift. This value is particularly useful for estimating transient P-Δ effects. However, the peak transient tilt and the peak transient story drift ratio are not necessarily coincident, so we recommend estimating the combined drift by the square-root-sum-of-squares method already commonly used for modal superposition.

MODEL APPLICABILITY AND LIMITATIONS

Applicability

We provide a distilled guide with recommendations for model implementation in this section. Table 9 summarizes the models and equations that may be used, depending on the details available to the analyst. Scenarios 1 and 2 in Table 9 predict tilt for structures when information about soil profile heterogeneity in plan is not available; those effects are captured by the model uncertainty because this condition is present

492 in the case histories used to develop these models. Scenario 3 deals with cases for which heterogeneity in
493 plan is observed and characterized. In this case, the results from scenario 2 (the semi-empirical model) are
494 compared to the results from using a model for foundation settlement to evaluate differential settlement due
495 to variations in soil properties across the foundation (and subsequently derive tilt). Finally, scenario 4 may
496 be of interest to engineers, because the coincidence of settlement and tilt may be critical for engineering
497 decision making. In this scenario, the probability distributions of residual tilt conditioned on settlement
498 have model uncertainty that is smaller yet. Example applications of all four scenarios are included in
499 Appendix II. In conjunction with the Bullock et al. (2018) settlement model, correlations provided can also
500 be used to determine the probability of exceedance of given settlement-tilt scenarios (e.g., settlement above
501 50 cm and tilt above 1.0 degree).

502 Based on any of the above estimates of residual tilt, the semi-empirical model for the transient tilt
503 ratio (Equation 10) can subsequently be applied to generate estimates of the peak transient tilt (Equation
504 12). The correlation coefficients provided can be used to determine the probability of exceedance of given
505 combinations of tilt values (e.g., residual tilt above 1.0 degree and peak transient tilt above 2.0 degrees).

506 **Model Limitations**

507 The models described above have several limitations. First, we expect the behavior of other foundation
508 systems to differ significantly from that of mats. Second, all models are only applicable to structures on
509 mat foundations with effective heights up to 15 m (or a true height of roughly 21m, about six stories). Limits
510 on other input parameters are not as critical to consider given the relative sensitivity of tilt predictions to
511 changes in effective height.

512 In addition, the empirical model for residual foundation tilt (Equation 1/Scenario 1) requires use of
513 a probabilistic model for foundation settlement. Therefore, the quality of predictions made using this model
514 cannot be separated from the assumptions, flaws, biases, or applicability restrictions of the co-implemented
515 settlement model. In addition, more information may be needed about site geometry and soil profiles if the
516 settlement model requires it. Finally, correctly estimating the uncertainty around predictions requires
517 estimates of correlation between the errors in predicting settlement and in predicting residual tilt. We

518 quantify the necessary correlations for use with the Bullock et al. (2018) settlement model, but more work
519 is needed to develop these coefficients for use with other settlement models (e.g., Unutmaz and Cetin 2012;
520 Bray and Macedo 2017; Lu 2017).

521 The semi-empirical model for residual foundation tilt (Equations 6&9-10/Scenarios 2-3 requires
522 detailed knowledge of a single borehole, which may be impractical for some projects. This model accounts
523 for inertial effects, localized volumetric strains, and the effects of vertical heterogeneity. The numerical and
524 centrifuge models used to begin the development of the semi-empirical model are shaken with one-
525 dimensional horizontal excitation, and, therefore, exclude effects that arise from complex,
526 multidimensional shaking. The influence of the multidimensional ground motion is only included in the
527 model insofar as it is present in the case history database. This model may also not fully capture effects of
528 correlations between certain soil, foundation and structural parameters. In particular, the numerical model
529 varied these parameters individually (i.e. treating them as uncorrelated). The centrifuge focused on more
530 realistic combinations of parameters but, due to the relatively simplistic representation of complex
531 structures at scale in the centrifuge, the correlation between certain parameters is weaker in the experiments
532 than observed in case histories. In particular, multicollinearity expected in the real world among structure
533 height, structure mass, and foundation bearing pressure may lead to poorly constrained model behavior for
534 very tall and massive structures. In addition, any effects from horizontal heterogeneity that influenced the
535 tilt observed in the case history database are reflected in the model uncertainty. If significantly
536 heterogeneous site conditions are observed and characterized, probabilistic models for settlement should be
537 used to form an alternative estimate of differential settlement as a comparison.

538 The empirical model for residual tilt and the final adjustment of the semi-empirical model for
539 residual tilt are based on a relatively limited case history database, and we therefore expect the estimates of
540 model uncertainty to be small. We suggest following the recommendations of FEMA P-58 (FEMA 2012)
541 to adjust model uncertainty, and the values presented in Table 9 include this adjustment. In addition, both
542 models for residual foundation tilt fail to explicitly consider structure-soil-structure interactions (SSSI) in

543 urban settings, which have been shown to affect tilt significantly (Hayden et al. 2015; Kirkwood and Dashti
544 2018). The influence of any SSSI exhibited in the case histories contributes to the model uncertainty.

545 The final adjustment to the semi-empirical model suggests that the residual tilt of buildings at sites
546 with more interlayering of susceptible and non-susceptible layers will generally be larger. Cubrinovski et
547 al. (2017) and Beyzaei et al. (2018) observed the opposite trend for surficial manifestations of liquefaction
548 and formation of ejecta at sites away from buildings in the Canterbury earthquakes. Further investigation
549 is required to determine whether the trend observed in this study is the result of: (1) the influence of
550 interlayering on void redistribution and therefore softening of the susceptible layers, or (2) a reversal in the
551 trend of ejection potential caused by the presence of the structure and nature of ground motions. Regardless,
552 the case histories currently available show a significant trend increasing tilt with proxies for vertical
553 heterogeneity, and neglecting this effect might result in unconservative estimates of foundation tilt.

554 The model for the transient tilt ratio is based on centrifuge data. As a result, the influence of
555 heterogeneous soil conditions (particularly in plan) on peak transient tilt are not incorporated. However, we
556 expect tilt due to heterogeneity to be irreversible, which would tend to reduce the transient tilt ratio to 1.0.
557 The model's estimates of the transient tilt ratio are therefore incomplete, but conservative. The model for
558 peak transient tilt is based on the transient tilt ratio and, hence, it is also susceptible to the limitations of the
559 models for residual tilt discussed above.

560 Although the models for residual tilt are unbiased with regard to the case history database, the small
561 size of the currently available database (i.e., 20 cases) may not completely represent all trends in the field.
562 This database is used primarily to adjust for the effects of vertical heterogeneity, and the influence of all
563 other parameters of the SFS system is characterized using the extensive numerical database and the
564 relatively larger centrifuge test database. Lastly, the case history database includes relatively few cases that
565 experienced small settlements (i.e., less than 10 cm), and the models may or may not be unbiased in these
566 cases. In addition, residual tilt occurred in all buildings in the existing case history database, so both the
567 empirical and semi-empirical models are conditioned on the occurrence of visible tilt, which may lead these
568 models to exhibit slight bias towards over-prediction. This implicit conditioning does not necessarily mean

569 that the models are conditioned on the triggering of liquefaction (i.e., the excess pore pressure ratio, r_u,
570 reaching 1.0), since significant softening and tilt can occur even if liquefaction does not initiate under the
571 building.

572 **CONCLUDING REMARKS**

573 This study presents empirical and semi-empirical probabilistic models for estimating the residual and peak
574 transient tilt of mat-founded structures on potentially liquefiable ground. The models account for the
575 influence of soil, foundation, and structure properties, and are consistent with current mechanistic
576 understanding of the phenomenon of liquefaction and its consequences.

577 The empirical model for residual tilt was developed based on case histories using forward stepwise
578 feature selection, and is a function of settlement. The lasso was used to determine optimum forms for the
579 semi-empirical model of residual tilt based on a large set of fully-coupled, 3D, dynamic numerical
580 simulations of soil-foundation-structure systems, subsequently adjusted according to centrifuge modeling.
581 The model was further validated and adjusted using the available case history database of actual building
582 settlements and residual tilts. The model for peak transient tilt was based on the ratio between the peak
583 transient and residual tilts as observed in the centrifuge experiments, which we defined as the transient tilt
584 ratio. These semi-empirical models are independent of any prediction of settlement.

585 Probabilistic estimates of residual tilt from these models improve our ability to predict losses due
586 to the demolition of structures that have experienced excessive tilt in the future. For example, structures
587 that experience tilt over a certain threshold may need to be demolished and replaced, and the peak transient
588 tilt may also lead to more severe structural damage. Likewise, probabilistic estimates of peak transient tilt
589 help predict possible amplification of P-Δ effects in the superstructure above these foundations.

590 Combined with probabilistic models for foundation settlement (Unutmaz and Cetin 2012; Bray and
591 Macedo 2017; Lu 2017; Bullock et al. 2018), these models for foundation tilt allow engineers to form a
592 more holistic understanding of the possible consequences of liquefaction for a given mat-founded building
593 on a given site, in terms of settlement and tilt. If combined with understanding of lateral spread, ground
594 oscillation, modification of ground motions, and the potential for deformations due to the formation of

water films, this information is critical for decision-making regarding mitigation for both new and existing structures.

ACKNOWLEDGMENTS

Support for this research was provided partly by the U.S. Department of Education under award number P200A150042, partly by the U.S. National Science Foundation (NSF) through grant number 145431, and partly by the Department of Civil, Environmental, and Architectural Engineering and the University of Colorado Boulder (CU). Any opinions, findings, and conclusions or recommendations expressed in this material are those of the authors and do not necessarily reflect the views of the funding organizations. The numerical simulations utilized the Janus supercomputer, which is supported by NSF (award number CNS-0821794) and CU. The Janus supercomputer is a joint effort of the CU Boulder, CU Denver, and the National Center for Atmospheric Research.

REFERENCES

Acacio, A. A., Kobayashi, Y., Towhata, I., Bautista, R. T. & Ishihara, K. (2001). Subsidence of building foundation resting upon liquefied subsoil: case studies and assessment. *Soils and Foundations* 41(6), 111–128.

Allmond, J. & Kutter, B. (2012). Centrifuge Testing of Rocking Foundations on Saturated and Submerged Sand: Centrifuge Data Report for JDA01. (Report No. UCD/CGMDR-12/01). University of California, Davis.

Allmond, J. & Kutter, B. (2013). Centrifuge Testing of Rocking Foundations on Saturated and Submerged Sand: Centrifuge Data Report for JDA02. (Report No. UCD/CGMDR-13/01). University of California, Davis.

Arlot, S. & Celisse, A. (2010). A survey of cross-validation procedures for model selection. *Statistics surveys* 4, 40–79.

Beyzaei, C. Z. (2017). Fine-Grained Soil Liquefaction Effects in Christchurch, New Zealand (Doctoral dissertation). University of California, Berkeley.

Beyzaei, C. Z., Bray, J. D., van Ballegooy, S., Cubrinovski, M., & Bastin, S. (2018). "Depositional environment effects on observed liquefaction performance in silt swamps during the Canterbury earthquake sequence." *Soil Dynamics and Earthquake Engineering*, 107, 303-321.

Boulanger, R.W. & Idriss, I. M. (2014). CPT and SPT based liquefaction triggering procedures. Technical Report Rep. No. UCD/CGM-14, 1.

Bray, J., Cubrinovski, M., Zupan, J. & Taylor, M. (2014). Liquefaction effects on buildings in the central business district of Christchurch. *Earthquake Spectra* 30(1), 85–109.

Bray, J. D., & Macedo, J. (2017). 6th Ishihara lecture: Simplified procedure for estimating liquefaction-induced building settlement. *Soil Dynamics and Earthquake Engineering*, *102*, 215-231.

Bray, J. D. & Sancio, R. B. (2006). Assessment of the liquefaction susceptibility of fine-grained soils. *Journal of Geotechnical and Geoenvironmental Engineering* 132(9), 1165–1177.

Bray, J. D. & Sancio, R. B. (2009). Earthquake geotechnical case histories for performance-based design, Ch. Performance of buildings in Adapazari during the 1999 Kocaeli, Turkey earthquake. CRC Press, pp. 325–340.

Bullock, Z., Dashti, S., Liel, A., Porter, K., Karimi, Z. & Bradley, B. (2017). Ground motion prediction equations for arias intensity, cumulative absolute velocity, and peak incremental ground velocity for rock sites in different tectonic environments. *Bulletin of the Seismological Society of America, 107(5)*, 2293-2309.

Bullock, Z., Karimi, Z., Dashti, S., Porter, K., Liel, A. B., & Franke, K. W. (2018). A Physics-Informed Semi-Empirical Probabilistic Model for the Settlement of Shallow-Founded Structures on Liquefiable Ground. *Geotechnique*. Under review.

Cetin, K. O., Bilge, H. T., Wu, J., Kammerer, A. M. & Seed, R. B. (2009). Probabilistic model for the assessment of cyclically induced reconsolidation (volumetric) settlements. *Journal of Geotechnical and Geoenvironmental Engineering* 135(3), 387–398.

Cetin, K. O., Unutmaz, B. & Jeremic, B. (2012). Assessment of seismic soil liquefaction triggering beneath building foundation systems. *Soil Dynamics and Earthquake Engineering* 43, 160–173.

Cubrinovski M, Bradley BA, Wotherspoon L, Green R, Bray J, Wood C, Pender M, Allen J, Bradshaw A, Rix G, Taylor M, Robinson K, Henderson D, Giorgini S, Ma K, Winkley A, & Zupan J. Geotechnical Aspects of the 22 February 2011 Christchurch earthquake. *Bulletin of the New Zealand Society of Earthquake Engineering, Special Issue on the 22 February 2011 Christchurch earthquake*, 2011, Vol 44 No 4, pp 181-194.

Cubrinovski M, Bray JD, Taylor M, Giorgini S, Bradley BA, Wotherspoon L, Zupan J. Soil liquefaction effects in the central business district during the February 2011 Christchurch earthquake. *Seismological Research Letters,* 2011*,* Vol. 82 No. 6, pp 893-904.

Cubrinovski, M., K. Ishihara, & T. Shibayama (2003). Seismic 3-D effective stress analysis: Constitutive modelling and application, Proc. *3rd Int. Conf. Deformation Characteristics of Geomaterials*, Lyon, France, 22–24 September 2003.

Cubrinovski M, Rhodes A, Ntritsos N, van Ballegooy S. "System response of liquefiable deposits." In: *Proceedings of the 3rd international conference on performance-based design in earthquake geotech. eng*., Vancouver, BC; 2017.

Dashti, S., Bray, J. D., Pestana, J. M., Riemer, M. R. & Wilson, D. (2010a). Centrifuge testing to evaluate and mitigate liquefaction induced building settlement mechanisms. Journal of Geotechnical and Geoenvironmental Engineering 136(7), 918–929.

Dashti, S., Bray, J. D., Pestana, J. M., Riemer, M. R. & Wilson, D. (2010b). Mechanisms of seismically-induced settlement of buildings with shallow foundations on liquefiable soil. Journal of Geotechnical and Geoenvironmental Engineering 136(1), 151–164.

Efroymson, M. A. (1960). Multiple regression analysis. *Mathematical methods for digital computers*, 191-203.

669 FEMA. (2012). Seismic performance assessment of buildings, volume I — methodology, FEMA P-58.
670 Federal Emergency Management Agency, Washington, D.C.

671 Hayden, C. P., Zupan, J. D., Bray, J. D., Allmond, J. D., & Kutter, B. L. (2015). Centrifuge Tests of
672 Adjacent Mat-Supported Buildings Affected by Liquefaction. *Journal of Geotechnical and*
673 *Geoenvironmental Engineering.* 141(3).

674 Holland, P. W., & Welsch, R. E. (1977). Robust regression using iteratively reweighted least-squares.
675 Communications in Statistics-theory and Methods, 6(9), 813-827.

676 Idriss, I. M. & Boulanger, R. W. (2008). Soil liquefaction during earthquakes. Oakland, CA: Earthquake
677 Engineering Research Institute.

678 Jampole, E., Deierlein, G., Miranda, E., Fell, B., Swensen, S., & Acevedo, C. (2016). Full-Scale
679 Dynamic Testing of a Sliding Seismically Isolated Unibody House. *Earthquake Spectra*, *32*(4),
680 2245-2270.

681 Karimi, Z., & Dashti, S. (2015). Numerical and centrifuge modeling of seismic soil-foundation-structure
682 interaction on liquefiable ground. *Journal of Geotechnical and Geoenvironmental Engineering*. 142(1),
683 04015061.

684 Karimi, Z., & Dashti, S. (2016). Seismic performance of shallow-founded structures on liquefiable ground:
685 Validation of numerical simulations using centrifuge experiments. *Journal of Geotechnical and*
686 *Geoenvironmental Engineering*. 142(6), 04016011.

687 Karimi, Z., Dashti, S., Bullock, Z., Porter, K. & Liel, A. (2018). Key predictors of structure settlement on
688 liquefiable ground: A numerical parametric study. *Soil Dynamics and Earthquake Engineering*, In Press.

689 Kirkwood, P., & Dashti, S. (2018). A Centrifuge Study of Seismic Structure-Soil-Structure Interaction on
690 Liquefiable Ground and the Implications for Structural Performance. *Earthquake Spectra* (In Press).

691 Kokusho, T. (2003). Current state of research on flow failure considering void redistribution in
692 liquefied deposits. *Soil Dynamics and Earthquake Engineering*, *23*(7), 585-603.

693 Lilliefors, H.W. (1967). On the Kolmogorov-Smirnov test for normality with mean and variance unknown.
694 *Journal of the American Statistical Association* 62(318), 399–402.

695 Liu, L. & Dobry, R. (1997). Seismic response of shallow foundation on liquefiable sand. J. Geotech.
696 Geoenviron. Eng. 123(6), 557–567.

697 Lu, C. W. (2017). A Simplified Calculation Method for Liquefaction-Induced Settlement of Shallow
698 Foundation. *Journal of Earthquake Engineering*, 1-21.

699 Malvick, E. J., Kutter, B. L., Boulanger, R. W., & Kulasingam, R. (2006). Shear localization due
700 to liquefaction-induced void redistribution in a layered infinite slope. *Journal of Geotechnical*
701 *and Geoenvironmental Engineering*, *132*(10), 1293-1303.

702 Maurer, B. W., Green, R. A., Cubrinovski, M., & Bradley, B. A. (2014). Evaluation of the liquefaction
703 potential index for assessing liquefaction hazard in Christchurch, New Zealand. *Journal of Geotechnical*
704 *and Geoenvironmental Engineering*, *140*(7), 04014032.

705 Meyerhof, G. G. (1957). Discussion on research on determining the density of sands. In Proc., *4th Int. Conf.*
706 *of Soil Mechanics and Foundation Engineering.* London, 3, 110.

707 NCEER. (1997). Proceedings of the NCEER Workshop on Evaluation of Liquefaction Resistance of Soils,
708 Edited by Youd, T.L., Idriss, I.M., Technical Report No. NCEER-97-0022, December 31, 1997.

709 Olarte, J., Paramasivam, B., Dashti, S., Liel, A. & Zannin, J. (2017). Centrifuge modeling of mitigation-
710 soil-foundation-structure interaction on liquefiable ground. *Soil Dynamics and Earthquake Engineering* 97,
711 304–323.

712 Paramasivam, Balaji, Shideh Dashti, and Abbie Liel, "Influence of Prefabricated Vertical Drains on the
713 Seismic Performance of Structures Founded on Liquefiable Soils", *ASCE Journal of Geotechnical and*
714 *Geeoenvironmental Engineering*, In Press, 2018.

715 Quigley MC, Bastin S, Bradley BA. Recurrent liquefaction in Christchurch, New Zealand during the
716 Canterbury earthquake sequence. *Geology,* 2013. Vol. 41, No 4, pp 419-422.

717 Ruiz-García, J., & Miranda, E. (2006). Evaluation of residual drift demands in regular multi-storey frames
718 for performance-based seismic assessment. *Earthquake Engineering & Structural dynamics*, *35*(13), 1609-
719 1629.

720 Skempton, A. W. (1986). Standard penetration test procedures and the effects in sands of overburden
721 pressure, relative density, particle size, ageing and overconsolidation. *Geotechnique*, 36(3), 425-447.

722 Skrondal, A. & Rabe-Hesketh, S. (2004). Generalized latent variable modeling: Multilevel, longitudinal,
723 and structural equation models. CRC Press, Boca Raton, FL.

724 Stone, M. (1974). Cross-validatory choice and assessment of statistical predictions. *Journal of the royal*
725 *statistical society. Series B (Methodological)*, 111-147.

726 Tibshirani, R. (1996). Regression shrinkage and selection via the lasso. *Journal of the Royal Statistical*
727 *Society. Series B (Methodological)*, 267-288.

728 Tokimatsu, K. & Seed, H. B. (1987). Evaluation of settlements in sands due to earthquake shaking. *Journal*
729 *of Geotechnical Engineering* 113(8), 861–878.

730 Unutmaz, B. & Cetin, K. O. (2010). Seismic performance of mat foundations on potentially liquefiable
731 soils after 1999 Turkey earthquakes. METU Soil Mechanics and Found. Eng. Research Center. Report No:
732 METU/GTENG 10/09-02.

733 Unutmaz, B. & Cetin, K. O. (2012). Post-cyclic settlement and tilting potential of mat foundations. *Soil*
734 *Dynamics and Earthquake Engineering* 43, 271–286.

735 Van Ballegooy, S., Malan, P., Lacrosse, V., Jacka, M. E., Cubrinovski, M., Bray, J. D., O'Rourke, T. D.,
736 Crawford, S. A., & Cowan, H. (2014). Assessment of liquefaction-induced land damage for residential
737 Christchurch. *Earthquake Spectra*, *30*(1), 31-55.

738 Wu, C. F. J. (1986). Jackknife, bootstrap and other resampling methods in regression analysis. *the Annals*
739 *of Statistics*, 1261-1295.

740 Yoshimi, Y. & Tokimatsu, K. (1977). Settlement of buildings on saturated sand during earthquakes. *Soils*
741 *and Foundations* 17(1), 23–38.

742 Youd, T. L., Idriss, I. M., Andrus, R. D., Arango, I., Castro, G., Christian, J. T. & ... Ishihara, K. (2001).
743 Liquefaction resistance of soils: summary report from the 1996 NCEER and 1998 NCEER/NSF workshops
744 on evaluation of liquefaction resistance of soils. *Journal of Geotechnical and Geoenvironmental*
745 *Engineering* 127(10), 817–833.

746

747

748 **Table 1.** Summary of the case history database.
749

Reference	Earthquake	Total no. cases	No. mat cases	No. mat cases with measured residual tilt
Yoshimi and Tokimatsu (1997)	Niigata, 1964	14	2	2
Acacio et al. (2001)	Luzon, 1990	17	0	0
Bray and Sancio (2009)	Kocaeli, 1999	3	3	2
Unutmaz and Cetin (2010)	Kocaeli and Düzce, 1999	27	27	16
Bertalot et al. (2013)	Maule, 2010	19	14	0
Bray et al. (2014)	Christchurch, 2011	4	0	0
	Total	**84**	**46**	**20**

750

751

752 **Table 2.** Possible features for the empirical model of residual tilt.
753

$\ln(S)$	F_{LPC}	q	$\ln(q)$	B	$\ln(B)$
h_{eff}	$\ln(h_{eff})$	M_{st}	$\ln(M_{st})$	D_f	$\ln(D_f)$
$H_{S,1}$	$\ln(H_{S,1})$	$D_{S,T}$	$\ln(D_{S,T})$	$\ln(CAV)$	$\ln(V_{gi})$

754

755

Table 3. Coefficient values for the empirical model.

Parameter	Value	Parameter	Value
a_1	0.509	B_1^*	12
a_2	-0.936	B_2^*	16
a_3	-0.102	$\sigma_{r^e,1}$	0.342
σ_{r^e}	0.287	$\sigma_{r^e,2}$	0.123
		$\rho_{\theta_{r^e},S}$	0.194

760 **Table 4.** Input parameters considered in the numerical parametric study and their ranges.
761

Input Parameter	Range considered
Relative density of susceptible layers, D_r	30% to 85%
Thickness of uppermost susceptible[a)] layer, $H_{S,1}$	1 m to 20 m
Thickness of non-susceptible crust, $D_{S,T}$[b)]	1 m to 10 m
Multiple loose to medium-dense sand layers	1, 2, or 3 layers
Presence of a low-permeability cap	Present or absent
Initial site period, T_{so}	0.27 s to 0.85 s
Foundation bearing pressure, q	39 kPa to 220 kPa
Foundation embedment depth, D_f	1 m to 5 m
Foundation width, B	4.5 m to 15 m
Foundation length-to-width ratio, L/B	1.0 to 10.0
Structure height-to-width ratio, H/B	0.3 to 2.3
Structure height, h_{eff} (with constant H/B)	2.6 m to 13.7 m
Structure inertial mass, M_{st}	5,000 kg to 2,472,000 kg
Structure vibration period, T_{st}	0.25 s to 2.0 s
Bedrock shear wave velocity, $V_{s,rock}$	760 m/s to 2000 m/s

762 a) Generally defined as saturated, non-plastic, cohesionless soils (e.g., Bray and Sancio 2006)
763 b) Measured from the ground surface.
764
765

766 **Table 5.** Values of intensity measures for the selected intensity levels in Figure 5, Figure 6, and Figure 7.
767

Intensity	CAV (cm/s)	PGA (cm/s^2)	D_{5-95} (s)
Low	167.2	51.8	10.7
Moderate	430.0	136.2	11.3
High	1,248.8	289.9	12.6

768

769

770 **Table 6.** Summary of the centrifuge experimental database with realistic (non-rigid) structures on
771 liquefiable soil deposits.
772

Reference	Number of data points
Allmond and Kutter (2012, 2013)	74
Dashti et al. (2010a,b)	18
Olarte et al. (2017)	10
Paramasivam et al. (2018)	3

773

774

775 **Table 7.** Coefficients for the semi-empirical model for residual tilt.
776

Parameter	Value	Parameter	Value
α_0	-4.353	α_{12}	0.234
α_1	-0.329	α_{13}	0.404
α_2	-0.252	γ_0	0.066
α_3	-0.036	γ_1	0.165
α_4	-0.430	κ_0	2.383
α_5	-0.121	κ_1	1.491
α_6	0.003	κ_2	-0.168
α_7	0.026	κ_3	-0.327
α_8	-0.082	κ_4	0.087
α_9	0.314	$\sigma_{r^{se}}$	0.548
α_{10}	0.472	$\rho_{\theta_r^{se},S}$	0.500
α_{11}	-0.020		

777

778

779 **Table 8.** Coefficients for the model predicting the transient tilt ratio (Equation 10).
780

Parameter	Value	Parameter	Value
δ_0	2.639	B_1^*	8
δ_1	-0.577	B_2^*	10
δ_2	-1.285	$\sigma_{R_T,1}$	0.474
δ_3	0.088	$\sigma_{R_T,2}$	0.244
σ_{R_T}	0.442	ρ_{θ_T,R_T}	-0.182

781

782

Table 9. Implementation guide for the models in this study according to the level of detail in site investigation.

Scenario	Description	Model	Equations	Model σ_{tot}*
1	Calculate residual tilt based on knowledge of general profile geometry, including the critical susceptible layer(s)	Empirical model for residual tilt	1; Bullock et al. (2018) or other model for settlement	0.50 if using Bullock et al. (2018) settlement model
2	Calculate residual tilt based on detailed knowledge of profile geometry and soil properties at one location at the site	Semi-empirical model for residual tilt	6, 9, and 10	0.55
3	Calculate residual tilt based on detailed knowledge of profile geometry and soil properties at multiple locations around the site	Larger of the two: 1) Semi-empirical model for residual tilt; 2) Probabilistic model for differential foundation settlement based on evaluating settlement for profile to each side of the foundation	6, 9, and 10; Bullock et al. (2018) or other model for settlement	0.55; depends on the selected settlement model
4	Calculate residual tilt given the occurrence of a certain average foundation settlement	Empirical model for residual tilt	1	0.30

* Values of σ_{tot} in this table have been adjusted according to the recommendations of FEMA P-58 Appendix H (i.e., SRSS of model uncertainty with 0.10; FEMA 2012) to reflect uncertainty due to limitations of the databases. If analyzing a case with characteristics not included in the databases (e.g., sloping sites, etc.), these values should be recalculated by SRSS with 0.25 to reflect the increased uncertainty.

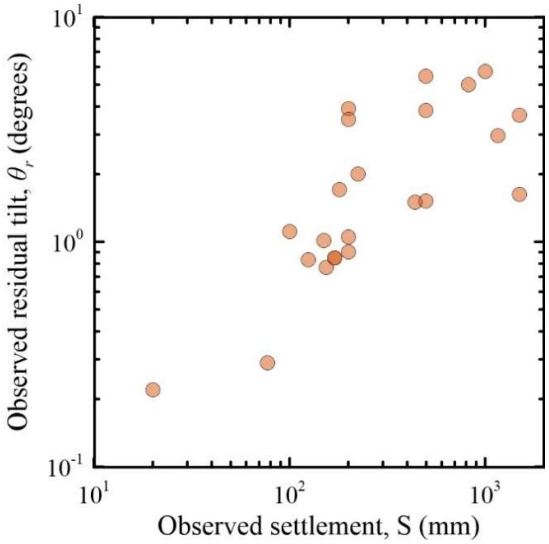

Figure 1. Average settlement and residual tilt for the case histories on mat foundations.

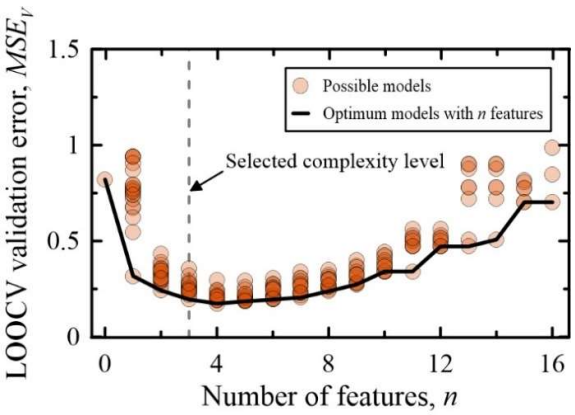

794
795 **Figure 2.** Validation error of models considered in greedy forward stepwise selection with 0 to 16
796 features.
797

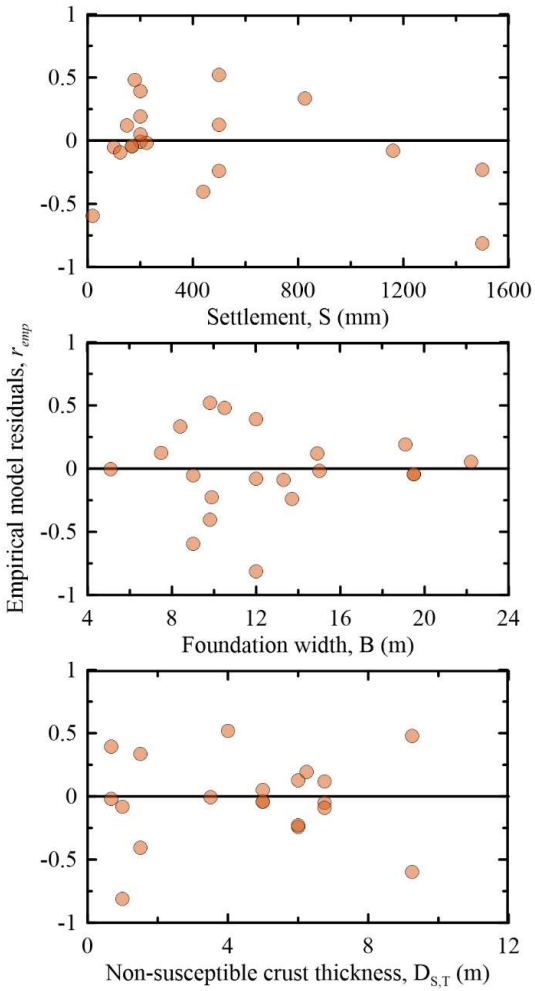

798
799 **Figure 3.** Residuals for the case history data using the empirical model (Equation 1).
800

801

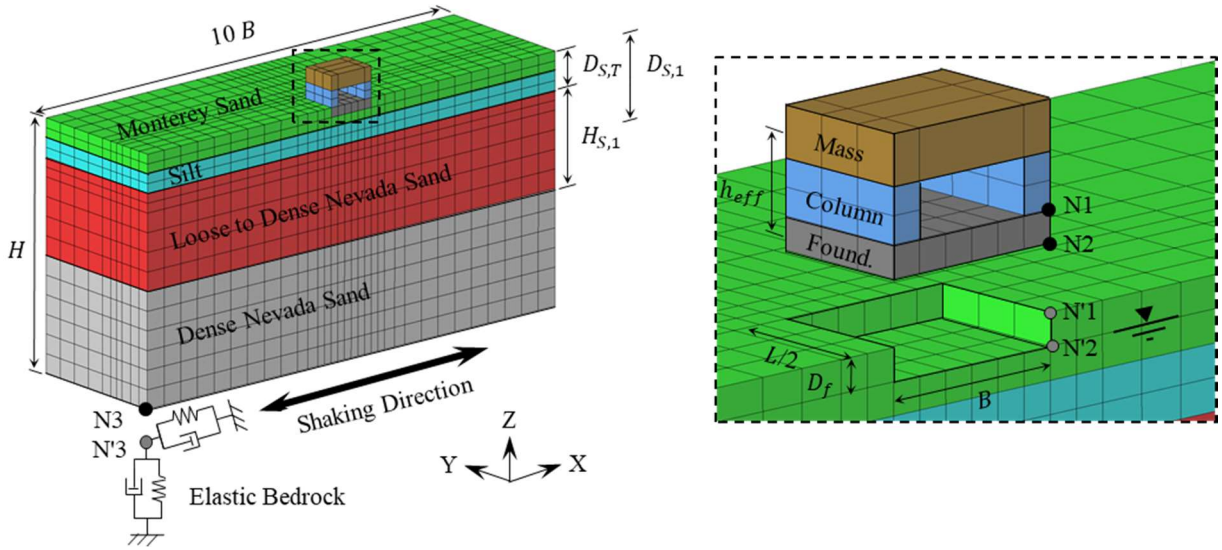

Figure 4. Schematic view of a numerical model from the parametric study.

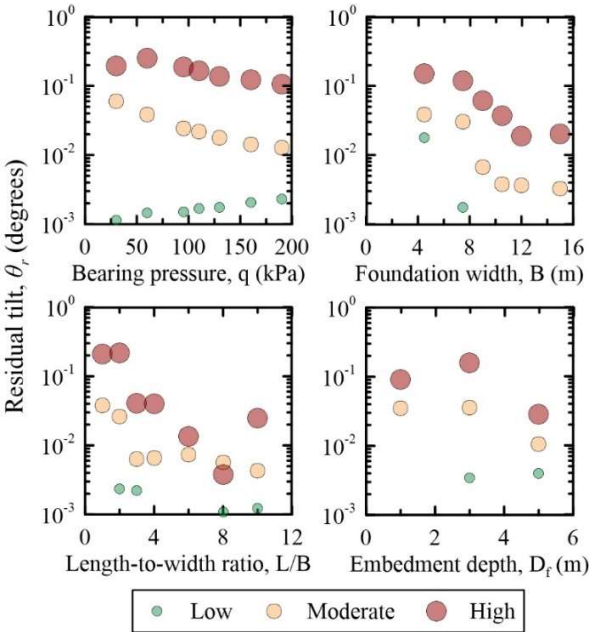

Figure 5. Sensitivity of residual tilt to properties of the foundation for three representative ground motions and intensity levels in numerical analyses.

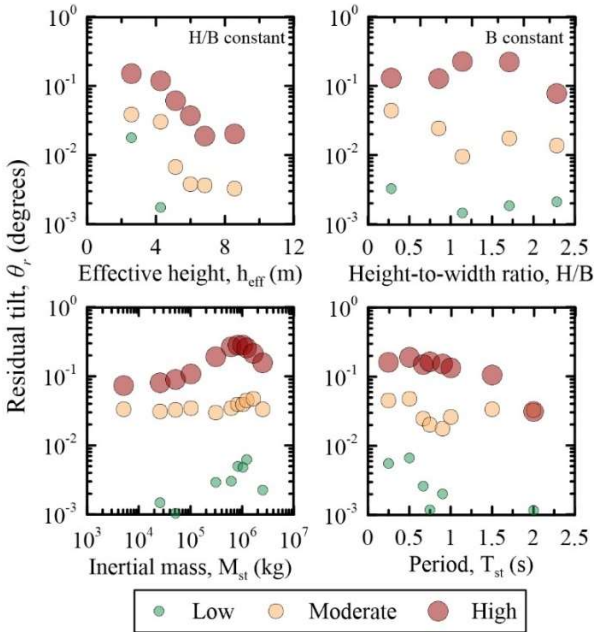

Figure 6. Sensitivity of residual tilt to properties of the structure for three representative ground motions and intensity levels in numerical analyses.

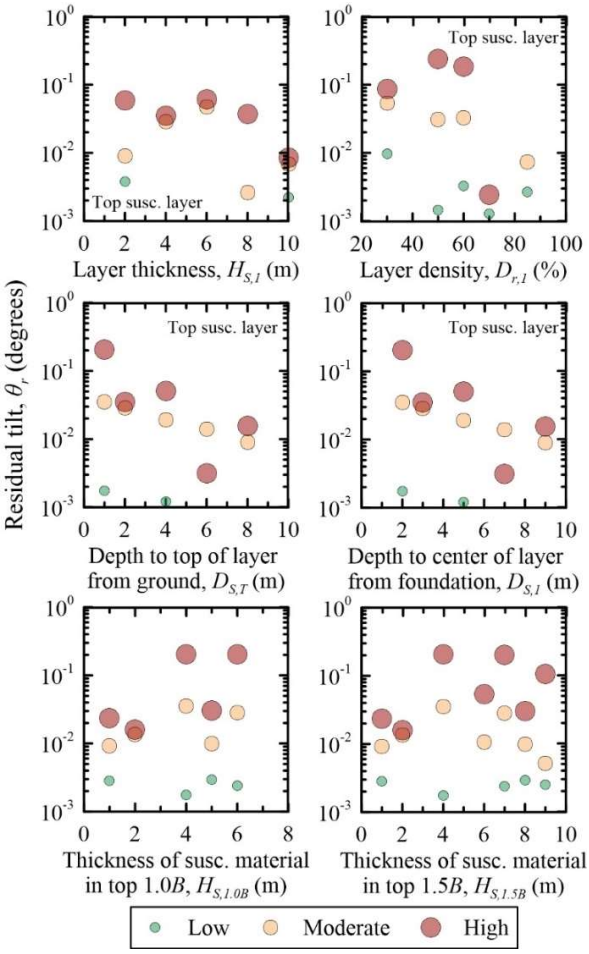

Figure 7. Sensitivity of residual tilt to properties of the soil profile for three representative ground motions and intensity levels in numerical analyses.

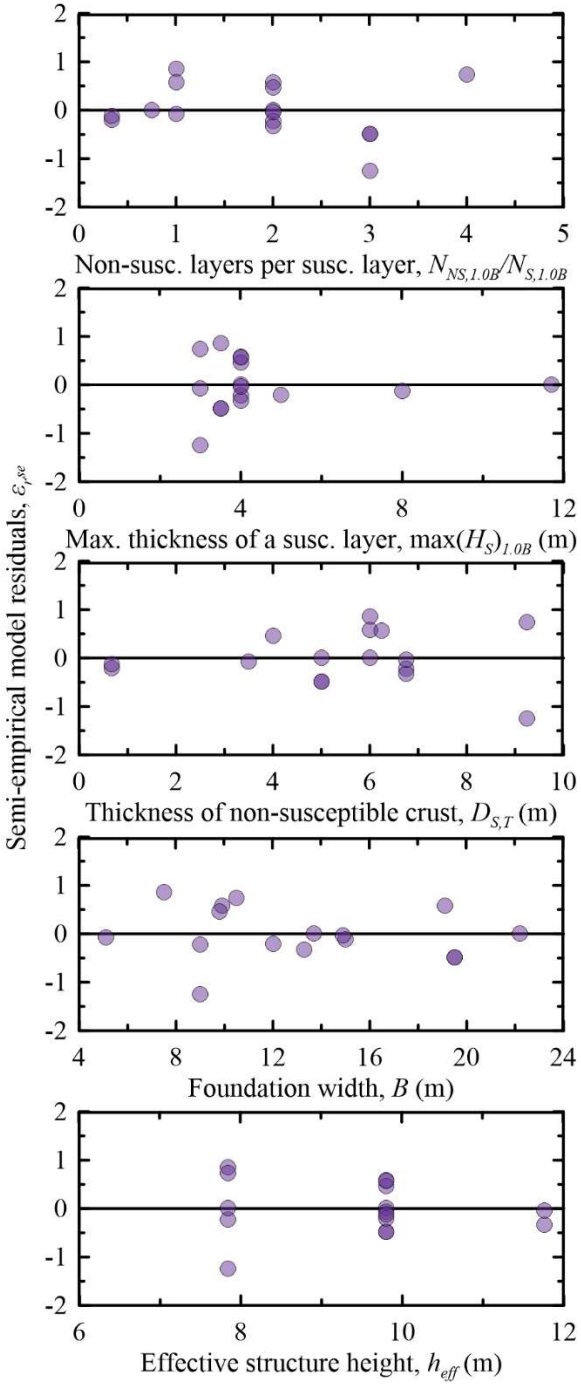

Figure 8. Adjusted residuals for the case history data using the semi-empirical model for residual tilt (Equations 6, 7, and 8).

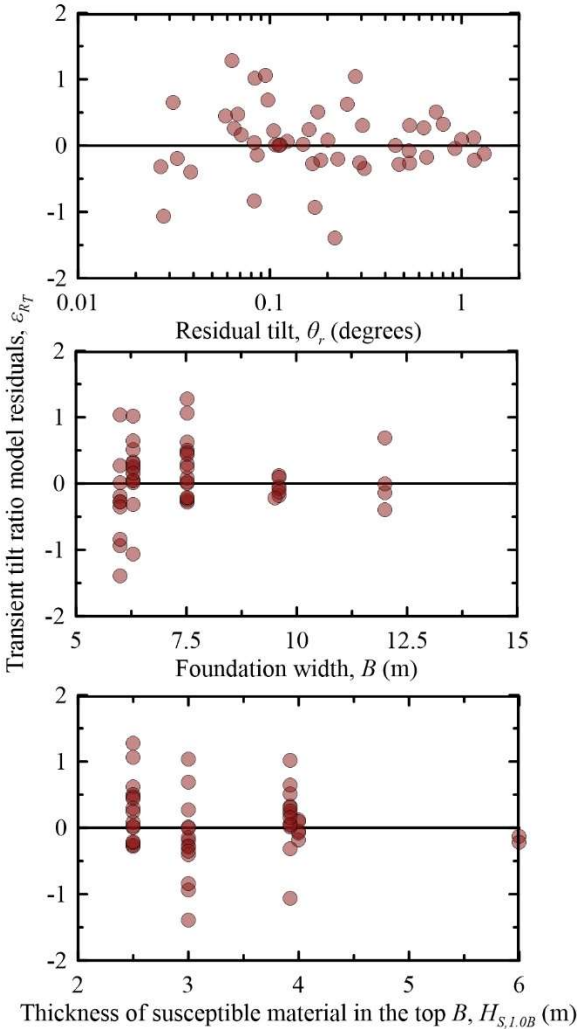

Figure 9. Residuals for the centrifuge data using the model for the transient tilt ratio (Equation 10).